World Journal of Advanced Research and Reviews
eISSN: 2581-9615 CODEN (USA): WJARAI
Cross Ref DOI: 10.30574/wjarr
Journal homepage: https://wjarr.com/

(REVIEW ARTICLE)

Check for updates

A review on tin dioxide gas sensor: The role of the metal oxide doping, nanoparticles, and operating temperatures

Jamal Malallah Rzaij *, Sameer Obaid Nawaf and Ahmed Khalil Ibrahim

Department of Physics, College of Science, University of Anbar, Ramadi, Iraq.

World Journal of Advanced Research and Reviews, 2022, 14(01), 051–062

Publication history: Received on 27 February 2022; revised on 30 March 2022; accepted on 01 April 2022

Article DOI: https://doi.org/10.30574/wjarr.2022.14.1.0288

Abstract

Metal oxide gas sensors have many advantages over other solid-state gas monitoring devices, including low cost, ease of manufacture, and small design. However, the shape and structure of sensing materials have a considerable impact on the performance of such sensors, posing a significant challenge for gas sensing properties on materials or dense films to attain high-sensitivity characteristics. Various tin dioxide (SnO_2) nanostructures have been devised to increase gas sensing characteristics such as sensitivity, selectivity, and response time, among other characteristics. An overview of the most well-known techniques for synthesizing gas-sensing films, as well as the influence of doping with various metal oxides, nanoparticle size, and operating temperature on the gas-sensing properties of such films, is discussed in this work. The gas sensing mechanisms and the gas detection techniques are presented in detail. The metal oxide doped SnO_2 showed a strong response for SO_2 and NO_2 gases, whereas nanoparticle doping plays a crucial effect in increasing SnO_2 sensitivity towards H_2, H_2S, NO_2, CO, Ethanol, etc. Furthermore, the effect of operating temperature on SnO_2 response is discussed in this report. SnO_2 has a high sensitivity over a wide temperature range (100-350 °C).

Keywords: Thin films; review; SnO_2; nanoparticles; doping effect; operating temperature

Graphical abstract

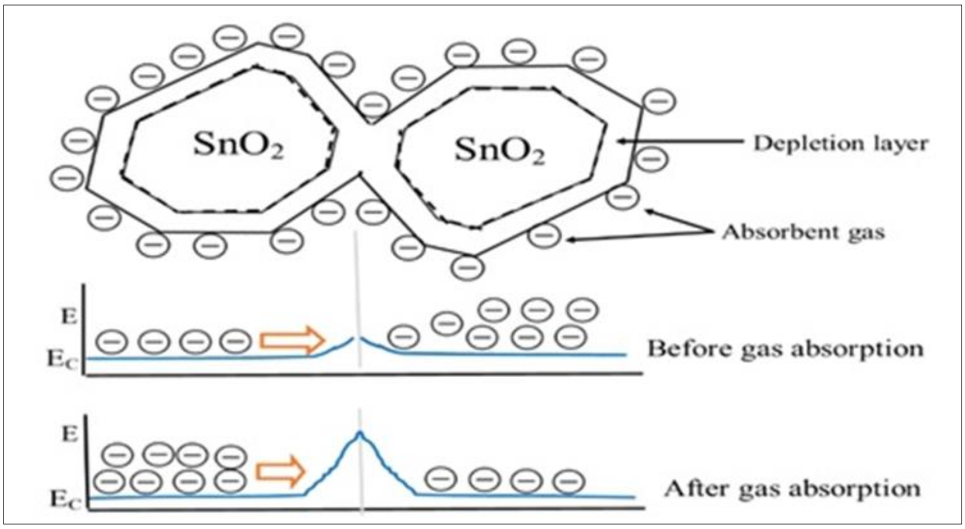

* Corresponding author: Jamal M. Rzaij
Department of Physics, College of Science, University of Anbar, Ramadi, Iraq.

1. Introduction

Nanoscience is described as the study of the properties of materials with nanometer-scale dimensions or the science concerned with tiny objects with dimensions ranging from a few nanometers to less than 100 nm [1]. Nanostructures metal oxides have a significant interest because of their size-dependent properties and their various applications [2]. Semiconductor oxides play a critical role in energy conservation and conversion applications, optoelectronics, memory applications, etc. [3–5]. One of the most critical types of semiconductors is the transparent conductive oxides (TCOs), which are composed of metal combined with oxygen, such as CdO, ZnO, and SnO_2 [6]. Such materials have two benefits; they are described by high electrical conductivity and optical transmittance. Despite the wide bandgap of these materials compared to the other semiconductors, the conduction band is full of free electrons. Thus, the transmittance spectrum within 400-1500 nm depends on the preparation conditions of the material.

Nanostructured semiconductors, such as SnO_2, ZnO, and TiO_2, can be used to detect a wide range of organic pollutants [7–11]. Tin (IV) Oxide (SnO_2) is an n-type transparent semiconductor with a wide bandgap of 3.6 eV at 300 K [12,13]. SnO_2 is used in a wide variety of applications, including photovoltaic devices [14–18], biological applications [19–23], solar cells [24–28], electrochemical applications [29–31], and gas sensors [32–37]. Due to its high sensitivity to reducing and oxidizing gases such as CO, H_2, and NO, tin oxide is commonly employed in gas sensor applications. [38]. It was prepared by several techniques such as sol-gel, microwave-assisted and ultrasound-assisted methods, solvothermal, pulsed laser deposition, solid-state reaction, microemulsion, hydrothermal deposition, electron beam evaporation, sonochemical, sputtering, spray pyrolysis, sonication, vapor-liquid-solid synthesis [26,29,39–45]. It is an inorganic compound with a density of 6.99 g/cm^3, and the melting point is 1624.85 °C [46].

The rutile is the most common crystal structure of SnO_2. It has a tetragonal unit cell with $P_{42/mm}$ (136) space group [47], and the lattice constants are a=b= 4.73 Å and c=3.18 Å [48]. A single unit cell includes six atoms, two of which are Tin and four Oxygen. Each Sn atom is surrounded by six O atoms at the octahedron's vertices in this structure, whereas three Sn atoms surround each O atom at an equatorial triangle's vertex.

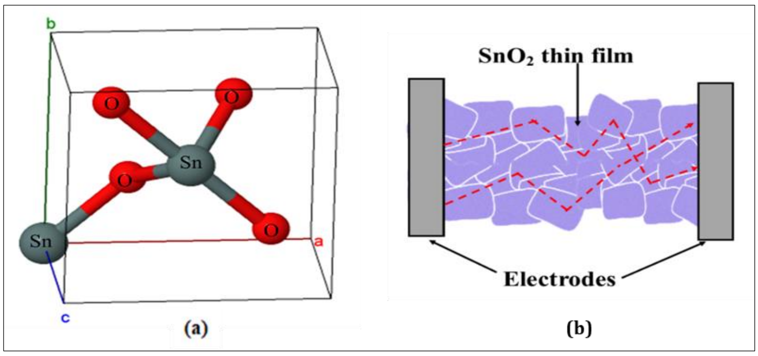

Figure 1 (a) Crystal structure of SnO_2 and (b) structure of SnO_2 thin film gas sensor

Figure 1(a) depicts the crystal structure of SnO_2. The particle size of SnO_2 nanostructures less than 20 nm with a surface area of 100-200 nm^2/g is particularly relevant in gas sensing applications. The structure of a SnO_2 thin film gas sensor is depicted in Figure 1(b). This review will highlight the most critical factors affecting the sensitivity of tin dioxide films and then compare the studied results from literature reviews to reach the optimal conditions for preparing tin oxide films as gas sensor devices.

2. Gas sensing mechanism

The detecting mechanism of metal-oxide gas sensors is based on species ionosorption on their surfaces, and the most significant ionosorbed species at ambient air are oxygen and water. The electrical and chemical activity of the O_2 vacancies on the surface of semiconductor oxides determines the sensing mechanism [49]. Two types of sensing reactions have been found in this mechanism. The first is the adsorb of charge-accepting molecules, such as oxygen or nitrogen dioxide, which extract the electrons from the conduction band at vacancy sites, decreasing the electrical conductance. Second, in an O_2 environment, oxygen molecules adsorbed on the surface react with gas molecules such as hydrogen or carbon dioxide, causing trapped electrons to be released and then injected back into the channel, increasing electrical conductivity [50]. The redox sensors' responses are categorized as oxidizing and reducing, which is the basis for decreasing and increasing channel conductance. Equations 1 and 2 illustrate the oxidizing response of the sensor:

$$NO + e^- \rightarrow NO^- \qquad (1)$$

While the reducing response of the sensor can be characterized by example:

$$CO + O \rightarrow CO_2 + e^- \qquad (2)$$

The temperature at which semiconductor sensors operate should be low enough to avoid long-term alterations to the bulk material and high enough that gas reactions occur in the order of the desired response time[51,52]. In general, semiconductor sensors that operate in relatively high-temperature ranges show a significant change in electrical resistance, which increases the rate of chemical reaction to the surface and thus increases the charge transfer processes [53]. The essential principle of semiconductor sensors working is dependent mainly on the interaction between the reactive chemical species (e.g., OH^-, O^-, O_2^-, and H^+) and the gas molecules to be sensed. The primary elements affecting semiconductor sensitivity are the microstructure (surface to volume ratio), the size of the grains, the thickness of the sensor film, and the pore size of the oxide particle [54].

3. Gas Detection Techniques

The quantum mechanical analysis demonstrated that the periodic crystal lattice sites restricted by the semiconductor surfaces produce localized surface states. When the energy levels of semiconductor material are in the forbidden energy region, the surface states may inject/trap electric charge into the bulk crystal. The crystal's ionized donors or acceptors generate a countercharge on the surface due to the corresponding surface charge. The band bending in the crystal is compatible with the formation of a double charge layer, which has a net negative charge and a positive countering charge in bulk [55].

The exposure of semiconductor surfaces, such as SnO_2 surface, to a gaseous atmosphere contributes to the development of more surface states as surrounding gases enhance the adsorption process occurring near the surface [56]. The principle of oxygen species adsorption, a component prevalent in most gas sensor applications, is illustrated in Figure 2a. The oxygen is adsorbed on the surface of the semiconductor when an electron is trapped from the conduction band, forming the oxygen ion O_2^-. This electron capture is the same as occupying a surface state generated by localized adsorption (O_2) [57]. Since the Fermi level of the semiconductor is higher than the surface state energy level in the absence of oxygen, this mechanism is possible. The charge transfer results in developing a surface charge and thus the bending of the semiconductor's band structure, as illustrated in Figure 2b. The Fermi level is dropped until enough oxygen has been adsorbed to equalize the surface energy level with the semiconductor Fermi level, referred to as Fermi level pinning. The bending of the tape results in the depletion of free surface charge carriers, the formation of a charge carrier depletion region, and then a high ohmic electrons resistance [55].

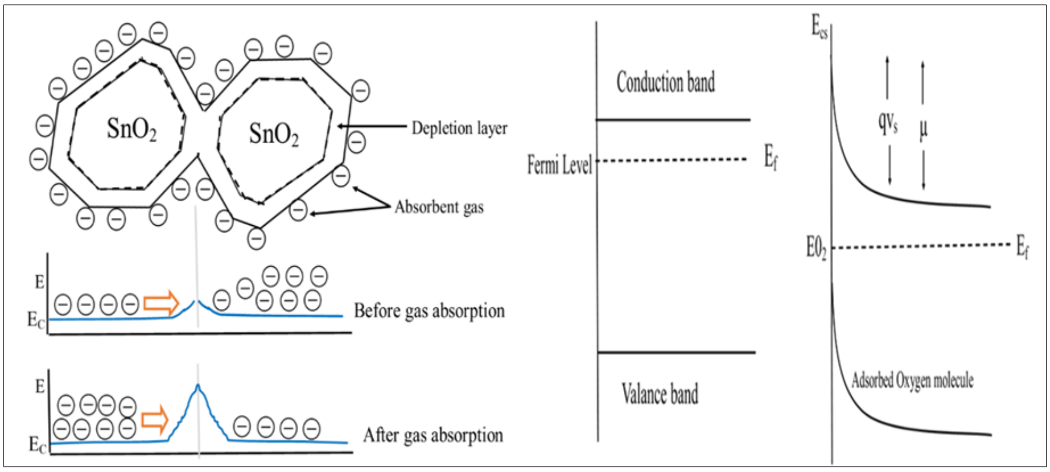

Figure 2 (a) The mechanism of SnO_2 thin film gas sensor and (b1) Diagram of valance band, conduction band, and Fermi level (b2) band bending in case of oxygen species adsorption on a sensor surface

4. Metal oxide doping effect

F. Ren et al. first reported that an excellent gas-sensitive performance of CuO/SnO_2 based sensor to BTEX belongs to the addition of catalyst CuO [58]. The highly sensitive, low-temperature, operated nitrogen dioxide (NO_2) gas sensor was fabricated using SnO_2 thin film doped with CuO. Sonker et al. stated that CuO/SnO_2 has a higher sensitivity than undoped SnO_2 [59]. Also, Zhou showed that p-type metal oxide (CuO) doped SnO_2 gas sensing thin films have high sensitive H_2S [60]. The CuO/SnO_2 thin film is confirmed to be a promising thin-film in gas sensor devices because the metal oxide catalyst increases the surface area. Punit Tyagi has studied the thin films' growth, especially SnO_2 thin films with high electrical resistivity, employing the NiO as a catalyst has combined on the surface of SnO_2 thin film with dotted nanoclusters and a continuous layer to enhance the response properties. The sensing response improved around 56 observed at a lower temperature for the NiO dotted cluster/SnO_2 sensor. Anjali Sharma has studied the structure of gas sensors based on RF sputtered SnO_2 thin film [61]. Various catalysts like In_2O_3, Al_2O_3, WO_3, CuO, NiO, and TeO_2 in nanoclusters structure have been deposited on the surface of SnO_2 to enhance the speed of response and recovery of the sensor and their effect on sensing response properties against NO_2 gas. According to D. Xue et al., the results of gas sensing demonstrate that the WO_3-SnO_2 nanocomposites have superior methane sensing properties compared to pure SnO_2 [62]. Punit Tyagi has presented the SO_2 gas sensing feature of SnO_2 thin film prepared using the RF sputtering method [63].

Various catalysts (MgO and V_2O_5) with nanoclusters form having a diameter of 600 μm have been loaded on the surface of SnO_2 for SO_2 gas detection. Both catalysts have incorporated with SnO_2 film, leading to high selectivity towards SO_2 gas at lower temperatures. J. Y. Choi and T. S. Oh described the sensor response of La_2O_3-doped SnO_2 to 10–75 ppm CO gas [64]. The La_2O_3-doped SnO_2 showed significantly improved CO sensitivity. Using the hydrothermal technique, S.Yan et al. prepared CeO_2-SnO_2 2-Dimensions nanosheets of equal size and little rhombus nanopores [65]. For the CeO_2-SnO_2 sensor, the response toward 100 ppm ethanol was 44, and it was larger two times than that of the pure SnO_2 sensor. In addition, the results showed that the CeO_2-SnO_2 nanosheets improved the characteristics of the gas sensing and the response and recovery time become shorter due to the effect of the CeO_2-doping and the porous structure.

Kuang-Chung Lee et al. studied the behavior of CO gas sensing of the PdO-decorated sensors by depositing the PdO nanoparticles on SnO_2 thin films via reactive sputter deposition [66]. For the PdO-decorated sensor, the sensor signal is larger than three times that of the pure SnO_2 sensor. Z.Tianshu et al. presented the CdO doping effect on conductance, microstructure, and gas-sensing characteristics of SnO_2-based sensors [67]. The 10 mol.% Cd-doped SnO_2-based sensor reveals the outstanding performance of ethanol-sensing, like a great sensitivity, is 275 for 100 ppm C_2H_5OH, great selectivity over CO, H_2, and i-C_4H_{10}, and a fast response rate of about 12 seconds for 90% response time. A comparison of the most common doping material summarizing its gas concentration and sensitivity is presented in Table (1).

Table 1 Comparison of the most common doping material summarizing gas type, gas concentration, and the sensitivity

Doping material	Gas	Gas Concentration ppm	Sensitivity%	Ref.
CuO	BTEX	50	6 times higher than pure	[58]
	NO_2	20	Highest response 1.83×10^2	[59]
	H_2S	-	Highest responses 438	[60]
WO_3	methane	500	2.3 times higher than pure	[62]
NiO	SO_2	500	Highest response ~ 56	[63]
La_2O_3	CO	50	Highest response 59.0	[64]
CeO_2	Ethanol	100	2 times higher than pure	[65]
PdO	CO	2000	1.6 times higher than pure	[66]
CdO	H_2	1000	Highest response at 98	[67]
NiO	SO_2	500	Maximum response ~ 56	[68]
WO_3	NO_2	10	Highest response 5.4×10^4	[69]
MgO, V_2O_5	SO_2	5000	317,166	[70]

5. Nanoparticles effect

P. Sun et al. synthesized the hierarchical Cd-doped and undoped SnO_2 nanostructures using the hydrothermal method's inexpensive and friendly environment [71]. The 3.0 wt.% Cd-doped SnO_2 based sensor exhibit outstanding selectivity toward H_2S. S. Rani reported the gas sensing properties of sol-gel-derived Fe-doped nanocrystalline SnO_2 thin films [72]. The films with 2% Fe content showed a high response and excellent selectivity for CO compared to other gases. Yanbai Shen et al. synthesized SnO_2 nanowires using a thermal evaporation method with a tetragonal structure [73]. The outcomes showed that the doping by Pd led to enhancing the sensor's response and decreased the operating temperature, which maximized the sensor's response. K. Hu et al. prepared Pd-doped SnO_2 nanofibers by magnetron and electrospinning sputtering [74]. The manufactured material showed a response of about 53 for 500 ppm hydrogen at the temperature of 130 °C, which is an essential enhancement compared with sensors untreated with plasma. J. Kaur prepared different kinds of thin films, indium-doped and undoped SnO_2 thin films with various values of doping concentrations by using the sol-gel spin coating technique on glass substrates [75].

At a low temperature, the indium doping improves the selectivity and sensor response towards NO_2 gas and prevents the agglomeration of particles, which is responsible for lowering the sensor response and stability in the range of particle size. As well, A. Salehi studied the dependence of the SnO_2 sensitivity on indium concentration by chemical vapor deposition [76]. The sensitivity of indium-doped SnO_2 is four times higher than the undoped sensor, which can be obtained for 1000 ppm methanol. M. D'Arienzo et al. carried out a one-pot install of SnO_2 and Pt–doped SnO_2 inverted opal thin films, which can be used for gas sensing [77]. The electrical sensitivity values under an atmosphere of CO/Air showed that the response of pure SnO_2 films is lower than Pt-doped films; also, the response of the sol–gel films is lower than inverted opal films. P. Ivanov used a valuable, thick-film technique to manufacture robust, small, and sensitive semiconductor metal oxide sensors to reveal traces of ethanol vapors in the air [78]. The alteration in resistance of the Pt-doped sensors is from two to fifty-five times larger than the alteration in the mercantile sensor. The material of Pt-doped SnO_2 is more sensitive, less resistant, and has a faster response to ethanol than that of pure SnO_2.

K. Y. Dong et al. fabricated nanofibers oxide gas sensors considered sensing materials on micro platforms by employing the micromachining technique [79]. The results showed that the responses of 0.08 wt.% Pt doped SnO_2 are more significant than that of pure SnO_2 nanofibers to 4–20 ppm H_2S. X. Kou et al. prepared pure SnO_2 nanofibers and 1–5 mol% Co-doped SnO_2 nanofibers using an electrospinning technique [80]. Their results revealed that the maximum response to 100 ppm ethanol was for 3 mol.% Co-doped SnO_2 nanofibers, about 40.1, four times greater than pure SnO_2 one. Using the spin-coating method, Kou Chong et al. prepared pure SnO_2 thin film and several thin films of 1–10 mol% Co-doped SnO_2 thin [80]. The result showed that the most response properties were for the sample of 1 mol% Co-doped SnO_2 thin film at a temperature of 225 °C, where the response was 59.04 with a response time of 7s toward 2000 ppm H_2 gas. The improved H_2 gas sensing properties are due to the smaller grain size and the formation of p-n heterojunction. Y. Guan et al. used a one-step hydrothermal route to prepare pure SnO_2 and Zn-doped SnO_2 hierarchical architectures [81]. The sensor-based on S3 (Zn^{2+}/Sn^{4+}=0.056) at the temperature of 213 °C exhibited outstanding selectivity toward ethanol with a response of about 14.4 to 100 ppm, achieving more than three times larger than the pure SnO_2 sensor. X. Ding prepared Zn-doped SnO_2 nanorods clusters for different sizes by modifying the concentration of Zn^{2+} in the solution by employing a facile hydrothermal method [82]. The morphology-composition-performance is the more the doping ratio of Zn, the longer the length of nanorods, and the larger the response to methanol, which is essential for the synthesis and the design of gas sensors with excellent performance.

P. S. Kolhe deposited SnO_2 based thin films on glass substrates with doped ratios 1.5, 3.0, and 4.5 mol% of Ag by employing the spray pyrolysis method [83]. A critical response (~ 1.38) with a short recovery and response time (110 s, 46 s) towards 450 ppm H_2S at a temperature of 100 °C can be observed for the sample with 3 mol.% Ag-doped SnO_2 film. X. Lian et al. have used the hydrothermal technique to manufacture pure and Ce-doped with 3, 5, and 7 wt.% SnO_2 nanoparticles. The outcomes have shown that the nanoparticles had formed of SnO_2 and Ce atoms had doped into the SnO_2 substrates, for 5 wt.% SnO_2:Ce, it has a greater specific surface area around 173.53 m^2/g. Significantly, the performance of the SnO_2:Ce sensor has enhanced contrasted to pure SnO_2 and showed the highest response, which is about 50.5 for 50 ppm, and good acetone selectivity at a temperature of 270 °C. A. I. Khudiar and A. M. Oufi doped SnO_2 thin films with Al thin films with concentrations of 0,1,3 and 5 % via the RF plasma sputtering technique [84]. The results show that the increase the doping levels to 3%, the response increases; however, for a doping concentration of 5%, the response decreases. Perfect properties of hydrogen sensing were obtained, such as good selectivity, fast response time, high response, and short recovery time. These results give good evidence that the additive enhances the gas sensor's performance. Y. Wu et al. synthesized single-crystal nanobelts of SnO_2 and La-SnO_2 (SnO_2 NBs, La-SnO_2 NBs) using thermal evaporation [85]. It found that at a concentration of 100 ppm, the single La-SnO_2 NB sensor had a high sensitivity of 8.76 toward ethanediol at an operating temperature of 230 °C.

C. M. Hung et al. synthesized ZnO-SnO_2 nanofibers doped with Au crystals by electrospinning technique for improving the performance of H_2S gas sensing [86]. Depending on the optimal doping concentration of Au, the gas sensitivity to H_2S is enhanced by around 700%. X. Kou et al. reported the effect of doping of Ru on the gas sensing characteristics of SnO_2 nanofibers for acetone detection [87]. The outcomes exhibit that the response to 100 ppm acetone of 2 mol% Ru-doped SnO_2 nanofibers is 118.8, larger than that of pure SnO_2. L. Du et al. synthesized undoped SnO_2 and Ga-doped porous micro flowers (SPMs) by a facile hydrothermal technique [88]. The sensor of 3 wt.% Ga-doped SPM shows a weak detection limit of 3.0/0.1 ppm and enhanced sensitivity of 95.8/50 ppm to formaldehyde at a temperature of 230 °C, which is greater than that of the pure SPM sensor at 21.2/50 ppm. Z. Jiang et al. synthesized a set of Eu-doped and undoped SnO_2 nanofibers by a simple electrospinning method and subsequent calcination treatment [89]. Eu-doped SnO_2 nanofibers show important improved sensing properties with short response and recovery time, considerable response value, and excellent selectivity to acetone vapor. Particularly, the sensor is based on 2 mol.% Eu-doped SnO_2 nanofibers demonstrate the highest response (32.2 for 100 ppm), which was two times greater than the pure SnO_2 sensor.

Inderan et al. fabricated an ethanol gas sensor using a hydrothermal technique with an improved sensor response using Ni-doped SnO_2 nanorods [90]. They demonstrated that the average length and diameter of the pure SnO_2 are 150 nm and 25 nm, respectively, while they were 35 nm and 6 nm for the 5.0Ni: SnO_2 nanorods; they are four times smaller than pure SnO_2 nanorods. They investigated that the high response of the 5.0Ni: SnO_2 nanorod sensor is due to the particle's dimensions, which leads to an increase in the charge depletion layer thickness and the existence of oxygen vacancies in the SnO_2 nanorods lattice elements. A comparison of the most common nanoparticle doping material summarizing its Gas Concentration and sensitivity is presented in Table (2).

Table 2 Comparison of the most common nanoparticle doping material summarizing gas type, gas concentration, and the sensitivity

Nanoparticle	Gas	Gas Concentration ppm	Sensitivity%	Ref.
Cd	H_2S	10-31	22 times higher than pure	[71]
Fe	NH_3, CO, C_2H_5OH	1000	46,120, 84	[72]
Pd	H_2	1000	Highest response 253	[73]
		500	Highest response 53.0	[74]
In	NO_2	500	Highest response 7200	[75]
	H_2	1000	4 times higher than pure	[76]
Pt	CO	580	One time higher than pure	[77]
	Ethanol	1-1000	2-55 times higher than pure	[78]
	H_2S	4-20	25.9–40.6 times higher than pure	[79]
Co	Ethanol	100	40.1	[80]
Zn	Ethanol	100	3.2 times higher than pure	[81]
	Methanol		Highest response 50.8	[82]
Ag	H_2S	450	Highest response 1.38	[83]
Al	H_2	50-500	3 times higher than pure	[84]
La	Ethanediol	100	Highest response 8.67	[85]
Au	H_2S	0.1-1	700	[86]
Ru	Acetone	100	12 times higher than pure	[87]
Ga	Formaldehyde	0.1-3.0	4.5 times higher than pure	[88]
Eu	Acetone vapor	100	2 times higher than pure	[89]
Ni	Ethanol	1000	13 times higher than pure	[90]
Co	H_2	2000	Highest response 59.04	[91]
Ce	Acetone	50	Highest response 50.5	[92]

6. Operating temperature effect

The operating temperature affects the sensitivity by increasing the chemical reaction speed between the components of the adsorbed oxygen and the gas molecules. At low temperatures, the sensor's response is determined by the speed of the chemical reactions, while the gas diffusion speed on the surface, at high temperatures. D. L. Kamble synthesized NO_2 gas sensor of nanocrystalline SnO_2 using different spray solution concentrations [93]. The prepared sensor achieved the responsivity of 556 when exposed to 40 ppm of NO_2 at an operating temperature of 150 °C with a response and recovery times of were 100-46 seconds and 48-224, respectively. Z. Ying synthesized nanowhiskers SnO_2 of mass production by evaporating Sn as powders at a temperature of 800 °C [94]. The SnO_2 nanowhiskers revealed that at a temperature of 300 °C, the sensitivity of ethanol gas was from 23 to 50 ppm. A. Alhadi et al. prepared SnO_2 nanoparticles by employing an inexpensive hydrothermal technique [95]. The pure SnO_2 nanoparticles sensor has excellent selectivity for 100 ppm ethanol at a temperature of 180 °C and the great response of about 27 s, and a weak detection of 5 ppm. In addition, it has a recovery time of about 2 s and a response time of about 4 s. The distinguish sensing characteristics of the SnO_2 sensor make it a suitable sensor for ethanol detection. G. D. Khuspe et al. synthesized SnO_2 nanostructure via an inexpensive sol-gel spin coating technique using the solvent m-cresol [96]. SnO_2 demonstrated the highest response (19%) of good stability, 77.90% toward 100 ppm NO_2 at an operating temperature of 200 °C. The recovery and response times (20 min and 7 sec) were also observed with the same operating parameters. Y. Shen formed SnO_2 nanowires on oxidized Si substrates by the thermal evaporation technique of Sn grains at 900 °C [73]. The sensitivity increased as the H_2 concentration increased, and the highest sensitivity (118) was observed for a 2wt.% Pt-doped SnO_2 sample when exposed to 1000 ppm H_2 at 100 °C.

Table 3 Comparison of the most common nanoparticle doping material summarizing its gas concentration, sensitivity, and temperature

Doping material	Gas	Gas Concentration ppm	Sensitivity%	Temperature^{0}C	Ref.
-	NO_2	40	Highest response at 556	150	[93]
-	Ethanol	50	Highest response at 23	300	[94]
-	Ethanol	100	Highest response at 27	180	[95]
Pd	LPG	5000	72%	350	[97]
Cu	H_2S	10	Highest response at 2500	100	[98]
	H_2S	100	1 time higher than pure	180	[99]
In	H_2	500-3000	7%	200	[100]
Co	H_2	100	Highest response at 24	330	[101]
-	NO_2	100	19%	200	[102]
Pt	H_2	1000	118	100	[103]

J. K. Srivastava analyzed the sensitivity, response, recovery time, and sensing mechanism of Pd-doped thick SnO_2 film for LPG detection [97]. The sensor doped with 1% palladium revealed the highest sensitivity of 72% at an operating temperature of 350 °C for 0.5% LPG concentration. C. M. Ghimbeu presented the possibility of electrostatic sprayed SnO_2 and SnO_2 doped with Cu films for NO_2, SO_2, and H_2S detection [98]. The doping significantly improves the sensing properties of SnO_2 films. Cu-doped SnO_2 films had a higher response against low H_2S concentrations (10ppm) at temperatures of 100°C. S. Zhang fabricated undoped and Cu-doped SnO_2 thin films with extensive specific surface areas via a self-assembled soft template combined with simple physical co-sputtering deposition [99]. The sensitivity of the undoped SnO_2 sensor is lesser than the Cu-doped SnO_2 porous sensor, with a recovery time ~ 42.4 sec and a response time ~10.1sec to 100 ppm of H_2S at a temperature of 180 °C. A. Salehi used Indium doping to improve the SnO_2 gas sensor selectivity [100]. Both indium-doped and undoped SnO_2 gas sensors were manufactured with various deposition methods. At various temperatures, ranging from 50 °C to 300 °C. The sensitivity change was measured for the sensors induced by selective gases of the hydrogen and wood smoke at concentrations ranging from 500 to 3000 ppm. The peaks of sensitivity of the samples show several values for selective gases with a response time of approximately 0.5 sec. L. Liu synthesized Pure and Co-doped SnO_2 nanofibers using an electrospinning technique [101]. Co-doped SnO_2

nanofibers reveal enhancing H_2 sensing characteristics. From the samples for pure and Co-doped SnO_2 nanofibers, it was found that 1 wt.% of Co-doped SnO_2 nanofibers exhibit the greatest response with a fast recovery and response times. When the sensor was exposed to100 ppm H_2 at 330 °C, the recovery time was 3 sec, and the response time was 2 sec, while the response was up to 24. A comparison of the most common nanoparticle doping material summarizing its Gas concentration, sensitivity, and temperature is presented in Table (3).

7. Conclusion

This paper reviews the effect of metal oxide doping, nanoparticles, and operating temperature on SnO_2 gas sensing characteristics towards numerous gases. Metal oxide catalyst increases the thin film's surface area, indicating that it can be used as a gas sensor. Doped/coated SnO_2 containing nanoclusters of various catalysts, such as In_2O_3, WO3, Cu, O, NiO and TeO_2, enhances the sensor response and recovery time and its sensitivity to a variety of gases. Doping SnO_2 with various semiconductors results in porous nanostructures that increase gas sensing features and shorten the response time and recovery time. The initial factor influencing particle dimensions (crystallite size and grain size), hence the thickness of the charge depletion layer and the presence of oxygen vacancies in the sensor lattice components, is doping with nanoparticles. Doping with nanoparticles at low temperatures improves the sensor's specific characteristics and response. The particle accumulation is responsible for lowering sensor response and stabilizing the particle size range. According to the reviews, Tin oxide is commonly employed in gas sensor applications due to its high sensitivity to reducing and oxidizing gases.

Compliance with ethical standards

Acknowledgments

The authors thank the Department of Physics, College of Science, University of Anbar, Iraq, for their direction, enthusiastic encouragement, and helpful critiques of this research study.

Disclosure of conflict of interest

The authors declare that there is no conflict of interest regarding the publication of this document.

References

[1] Shahzad N, Ali N, Shahid A, Khan S, Alrobei H. Synthesis of tin oxide nanoparticles in order to study its properties. Dig J Nanomater Biostructures. 2021; 16(1): 41–9.

[2] Winyayong A, Wongsaprom K. Nanostructures of tin oxide by a simple chemical route: Synthesis and characterization. J Phys Conf Ser. 2019; 1380(1): 8–12.

[3] Al-Jumaili BE, Rzaij JM, Ibraheam AS. Nanoparticles of CuO thin films for room temperature NO_2 gas detection: Annealing time effect. Mater Today Proc. Feb 2021; 42: 2603–8.

[4] Rzaij JM, Ibraheam AS, Abass AM. Cobalt Effect on the Growth of Cadmium Oxide Nanostructure Prepared by Spray Pyrolysis Technique. Baghdad Sci J. 1 Jun 2021; 18(2): 401–8.

[5] Kochuveedu ST, Jang YH, Kim DH. A study on the mechanism for the interaction of light with noble metal-metal oxide semiconductor nanostructures for various photophysical applications. Chem Soc Rev. 2013; 42(21): 8467–93.

[6] Al-Hashem M, Akbar S, Morris P. Role of Oxygen Vacancies in Nanostructured Metal-Oxide Gas Sensors: A Review. Sensors Actuators B Chem. 2019; 301: 126845.

[7] Kumari V, Yadav S, Mittal A, Kumari K, Mari B, Kumar N. Surface Plasmon response of Pd deposited ZnO/CuO nanostructures with enhanced photocatalytic efficacy towards the degradation of organic pollutants. Inorg Chem Commun. 2020; 121: 108241.

[8] He Z, Zhou J. Synthesis, Characterization, and Activity of Tin Oxide Nanoparticles: Influence of Solvothermal Time on Photocatalytic Degradation of Rhodamine B. Mod Res Catal. 2013; 2(3): 13–8.

[9] Liu H, Du C, Li M, Zhang S, Bai H, Yang L, et al. One-Pot Hydrothermal Synthesis of SnO_2/BiOBr Heterojunction Photocatalysts for the Efficient Degradation of Organic Pollutants under Visible Light. ACS Appl Mater Interfaces. 2018; 10(34): 28686–94.

[10] Ramirez R, Arellano C, Varia J, Martinez S. Visible Light-Induced Photocatalytic Elimination of Organic Pollutants by TiO_2: A Review. Curr Org Chem. 2015; 19(6): 540–55.

[11] Sanakousar FM, Vidyasagar C, Jiménez-Pérez VM, Prakash K. Recent progress on visible-light-driven metal and non-metal doped ZnO nanostructures for photocatalytic degradation of organic pollutants. Mater Sci Semicond Process. 2022; 140: 106390.

[12] Omar K. Tin Oxide Nanoparticles: Synthesis, Characterization and Study their Particle Size at Different Current Density. ARO, Sci J Koya Univ. 2013; 1(1): 17–21.

[13] Boran F, Çetinkaya S, Şahin M. Effect of surfactant types on the size of tin oxide nanoparticles. Acta Phys Pol A. 2017; 132(3): 546–8.

[14] Park NG, Kang MG, Ryu KS, Kim KM, Chang SH. Photovoltaic characteristics of dye-sensitized surface-modified nanocrystalline SnO_2 solar cells. J Photochem Photobiol A Chem. 2004; 161(2–3): 105–10.

[15] Kim H, Kushto GP, Auyeung RCY, Piqué A. Optimization of F-doped SnO_2 electrodes for organic photovoltaic devices. Appl Phys A Mater Sci Process. 2008; 93(2): 521–6.

[16] Sethi R, Ahmad S, Aziz A, Siddiqui AM. Structural, optical and electrical properties of tin oxide thin films for application as a wide band gap semiconductor. In: AIP Conference Proceedings. 2015. p. 030039.

[17] Smith JA, Game OS, Bishop JE, Spooner ELK, Kilbride RC, Greenland C, et al. Rapid Scalable Processing of Tin Oxide Transport Layers for Perovskite Solar Cells. ACS Appl Energy Mater. 2020; 3(6): 5552–62.

[18] Valaski R, Lessmann R, Roman LS, Hümmelgen IA, Mello RMQ, Micaroni L. Poly(3-methylthiophene)-based photovoltaic devices prepared onto tin-oxide/sulfonated-polyaniline electrodes. Electrochem commun. 2004; 6(4): 357–60.

[19] Lyau J-B, Wu H-C, Chen H. Biological studies with tin oxide materials. In: Tin Oxide Materials. Elsevier; 2020. p. 599–613.

[20] Singh AV, Jahnke T, Xiao Y, Wang S, Yu Y, David H, et al. Peptide-Induced Biomineralization of Tin Oxide (SnO 2) Nanoparticles for Antibacterial Applications . J Nanosci Nanotechnol. 2019; 19(9): 5674–86.

[21] Mohan AN, B M, Panicker S. Facile synthesis of graphene-tin oxide nanocomposite derived from agricultural waste for enhanced antibacterial activity against Pseudomonas aeruginosa. Sci Rep. 2019; 9(1): 1–12.

[22] Vijayalakshmi RV, Kuppan R, Kumar PP. Investigation on the impact of different stabilizing agents on structural, optical properties of Ag@SnO_2 core - shell nanoparticles and its biological applications. J Mol Liq. 2020; 307: 112951.

[23] Selvi Isabel AP, Kao CH, Mahanty RK, Wu YCS, Li CY, Lin CY, et al. Sensing and structural properties of Ti-doped tin oxide (SnO_2) membrane for bio-sensor applications. Ceram Int. 2017; 43(13): 10386–91.

[24] Liu D, Wang Y, Xu H, Zheng H, Zhang T, Zhang P, et al. SnO_2-Based Perovskite Solar Cells: Configuration Design and Performance Improvement. Sol RRL. 2019; 3(2): 1–22.

[25] Dahl PI, Barnett AO, Monterrubio FA, Colmenares LC. The use of tin oxide in fuel cells. In: Tin Oxide Materials. Elsevier; 2020. p. 379–410.

[26] Marikkannan M, Vishnukanthan V, Vijayshankar A, Mayandi J, Pearce JM. A novel synthesis of tin oxide thin films by the sol-gel process for optoelectronic applications. AIP Adv. 2015; 5(2): 0–8.

[27] Anaraki EH, Kermanpur A, Steier L, Domanski K, Matsui T, Tress W, et al. Highly efficient and stable planar perovskite solar cells by solution-processed tin oxide. Energy Environ Sci. 2016; 9(10): 3128–34.

[28] Xiong L, Guo Y, Wen J, Liu H, Yang G, Qin P, et al. Review on the Application of SnO 2 in Perovskite Solar Cells. Adv Funct Mater. 2018; 28(35): 1802757.

[29] Haq S, Rehman W, Waseem M, Shah A, Khan AR, Rehman MU, et al. Green synthesis and characterization of tin dioxide nanoparticles for photocatalytic and antimicrobial studies. Mater Res Express. 2020; 7(2): 025012.

[30] Nurzulaikha R, Lim HN, Harrison I, Lim SS, Pandikumar A, Huang NM, et al. Graphene/SnO_2 nanocomposite-modified electrode for electrochemical detection of dopamine. Sens Bio-Sensing Res. 2015; 5(June): 42–9.

[31] Dutta D, Chandra S, Swain AK, Bahadur D. SnO_2 quantum dots-reduced graphene oxide composite for enzyme-free ultrasensitive electrochemical detection of urea. Anal Chem. 2014; 86(12): 5914–21.

[32] Gaskov A, Rumyantseva M, Marikutsa A. Tin oxide nanomaterials: Active centers and gas sensor properties. In: Tin Oxide Materials. Elsevier; 2020. p. 163–218.

[33] Kolmakov A, Zhang Y, Cheng G, Moskovits M. Detection of CO and O_2 using tin oxide nanowire sensors. Adv Mater. 2003; 15(12): 997–1000.

[34] Viswanathan P, Patel AK, Pawar J, Patwardhan A, Henry R. Fabrication of Tin Oxide Nanoparticles for CO_2 Gas Sensing Layer. IETE J Res. 2020; 66(4): 460–5.

[35] Krishnakumar T, Jayaprakash R, Singh VN, Mehta BR, Phani AR. Synthesis and characterization of tin oxide nanoparticle for humidity sensor applications. J Nano Res. 2008; 4(2008): 91–101.

[36] Das S, Jayaraman V. SnO_2: A comprehensive review on structures and gas sensors. Prog Mater Sci. 2014; 66: 112–255.

[37] Abduljabbar QA, Radwan HA, Marei JM, Rzaij JM. Spray rate effects on the NO_2 gas sensor properties of Ni-doped SnO_2 nanoflakes. Eng Res Express. 1 Mar 2022; 4(1): 015028.

[38] Feng YS, Zhou SM, Li Y, Li CC, Zhang LD. Synthesis and characterization of tin oxide nanoparticles dispersed in monolithic mesoporous silica. Solid State Sci. 2003; 5(5): 729–33.

[39] Zhang J, Gao L. Synthesis and characterization of nanocrystalline tin oxide by sol-gel method. J Solid State Chem. 2004; 177(4–5): 1425–30.

[40] Khoiro M, Hashishin T, Muntini MS, Pramono YH. Morphological and optical properties of tin oxide nanomaterial thin film deposited using vacuum evaporation. J Ceram Soc Japan. 2020; 128(3): 158–63.

[41] Nagirnyak S V., Lutz VA, Dontsova TA, Astrelin IM. Synthesis and Characterization of Tin(IV) Oxide Obtained by Chemical Vapor Deposition Method. Nanoscale Res Lett. 2016; 11(1): 343.

[42] Senthilkumar V, Vickraman P, Ravikumar R. Synthesis of fluorine doped tin oxide nanoparticles by sol-gel technique and their characterization. J Sol-Gel Sci Technol. 2010; 53(2): 316–21.

[43] Rajesh N, Kannan JC, Krishnakumar T, Leonardi SG, Neri G. Sensing behavior to ethanol of tin oxide nanoparticles prepared by microwave synthesis with different irradiation time. Sensors Actuators, B Chem. 2014; 194: 96–104.

[44] Baco S, Chik A, Md. Yassin F. Study on Optical Properties of Tin Oxide Thin Film at Different Annealing Temperature. J Sci Technol. 2012; 4(1): 61–71.

[45] Cho S-M, Hong C-Y, Park S-Y, Lee D-S, Choi J-H, Koo B, et al. Application of Sulfated Tin (IV) Oxide Solid Superacid Catalyst to Partial Coupling Reaction of α-Pinene to Produce Less Viscous High-Density Fuel. Energies. 2019; 12(10): 1905.

[46] Orlandi MO. Tin oxide materials. In: Tin Oxide Materials. Elsevier; 2020. p. 1–9.

[47] Savioli J, Gavin AL, Lucid AK, Watson GW. The structure and electronic structure of tin oxides. In: Tin Oxide Materials. Elsevier; 2020. p. 11–39.

[48] Govaerts K, Partoens B, Lamoen D. Extended homologous series of Sn–O layered systems: A first-principles study. Solid State Commun. 2016; 243(i): 36–43.

[49] Marei JM, Khalefa AA, Abduljabbar QA, Rzaij JM. Nitrogen Dioxide Gas Sensor of In_2O_3- ZnO Polyhedron Nanostructures Prepared by Spray Pyrolysis. J Nano Res. 25 Oct 2021; 70: 41–51.

[50] Lu JG, Chang P, Fan Z. Quasi-one-dimensional metal oxide materials—Synthesis, properties and applications. Mater Sci Eng R Reports. May 2006; 52(1–3): 49–91.

[51] Ionescu R, Espinosa EH, Leghrib R, Felten A, Pireaux JJ, Erni R, et al. Novel hybrid materials for gas sensing applications made of metal-decorated MWCNTs dispersed on nanoparticle metal oxides. Sensors Actuators, B Chem. 2008; 131(1): 174–82.

[52] Korotcenkov G. Metal oxides for solid-state gas sensors: What determines our choice? Mater Sci Eng B Solid-State Mater Adv Technol. 2007; 139(1): 1–23.

[53] Zhang J, Liu X, Neri G, Pinna N. Nanostructured Materials for Room-Temperature Gas Sensors. Adv Mater. 2016; 28(5): 795–831.

[54] Ibrahim IM, Jamal M. Rzaij, Ramizy A. CHARACTERIZATION OF CuPcTs/PS for NO_2 GAS SENSOR. Dig J Nanomater Biostructures. 2017; 12(4): 1187–96.

[55] Bläser G, Rühl T, Diehl C, Ulrich M, Kohl D. Nanostructured semiconductor gas sensors to overcome sensitivity limitations due to percolation effects. Phys A Stat Mech its Appl. Apr 1999; 266(1–4): 218–23.

[56] Rzaij JM, Ali IM, Ibrahim IM. EFFECT OF Ce DOPED ON THE STRUCTURAL , OPTICAL , ELECTRICAL AND SENSING PROPERTIES OF V_2O_5 THIN FILMS PREPARED BY CHEMICAL SPRAY PYROLYSIS. Glob J Eng Sci Res. 2016; 3(1): 26–38.

[57] Khalefa AA, Marei JM, Radwan HA, Rzaij JM. In_2O_3-CuO NANO-FLAKES PREPARED BY SPRAY PYROLYSIS FOR GAS SENSING APPLICATION. Dig J Nanomater Biostructures. 2021; 16(1): 197–204.

[58] Ren F, Gao L, Yuan Y, Zhang Y, Alqrni A, Al-Dossary OM, et al. Enhanced BTEX gas-sensing performance of CuO/SnO_2 composite. Sensors Actuators, B Chem. 2016; 223: 914–20.

[59] Sonker RK, Sharma A, Tomar M, Yadav BC, Gupta V. Nanocatalyst (Pt, Ag and CuO) doped SnO_2 thin film based sensors for low temperature detection of NO_2 gas. Adv Sci Lett. 2014; 20(7–8): 1374–7.

[60] Zhou D, Gan L, Gong S, Fu Q, Liu H. P-type metal oxide doped SnO_2 thin films for H2S detection. Sens Lett. 2011; 9(2): 651–4.

[61] Sharma A, Tomar M, Gupta V. Enhanced response characteristics of SnO_2 thin film based NO_2 gas sensor integrated with nanoscaled metal oxide clusters. Sensors Actuators, B Chem. 2013; 181(2): 735–42.

[62] Xue D, Wang Y, Cao J, Sun G, Zhang Z. Improving methane gas sensing performance of flower-like SnO_2 decorated by WO_3 nanoplates. Talanta. 2019; 199(March): 603–11.

[63] Tyagi P, Sharma A, Tomar M, Gupta V. SnO_2 thin film sensor having NiO catalyst for detection of SO_2 gas with improved response characteristics. Vol. 248, Sensors and Actuators, B: Chemical. Elsevier B.V. 2017; 998–1005.

[64] Choi JY, Oh TS. CO sensitivity of La_2O_3-doped SnO_2 thick film gas sensor. Thin Solid Films. 2013; 547: 230–4.

[65] Yan S, Liang X, Song H, Ma S, Lu Y. Synthesis of porous CeO_2-SnO_2 nanosheets gas sensors with enhanced sensitivity. Ceram Int. 2018; 44(1): 358–63.

[66] Lee KC, Chiang YJ, Lin YC, Pan FM. Effects of PdO decoration on the sensing behavior of SnO_2 toward carbon monoxide. Sensors Actuators, B Chem. 2016; 226: 457–64.

[67] Tianshu Z, Hing P, Li Y, Jiancheng Z. Selective detection of ethanol vapor and hydrogen using Cd-doped SnO_2-based sensors. Sensors Actuators, B Chem. 1999; 60(2): 208–15.

[68] Tyagi P, Sharma A, Tomar M, Gupta V. Efficient detection Of SO_2 gas using SnO_2 based sensor loaded with metal oxide catalysts. Procedia Eng. 2014; 87(11): 1075–8.

[69] Sharma A, Gupta V, Tomar M. 8.3.4 Improved response characteristics of SnO_2 film based NO_2 gas sensor with nanoscaled metal oxide catalysts. 2020; (2): 702–5.

[70] Tyagi P, Sharma A, Tomar M, Gupta V. Effect of MgO and V 2 O 5 Catalyst on the Sensing Behaviour of Tin Oxide Thin Film for SO 2 Gas . Conf Pap Sci. 2014; 1–4.

[71] Sun P, Zhou X, Wang C, Wang B, Xu X, Lu G. One-step synthesis and gas sensing properties of hierarchical Cd-doped SnO_2 nanostructures. Sensors Actuators, B Chem. 2014; 190: 32–9.

[72] Rani S, Roy SC, Bhatnagar MC. Effect of Fe doping on the gas sensing properties of nanocrystalline SnO_2 thin films. Sensors Actuators, B Chem. 2007; 122(1): 204–10.

[73] Shen Y, Yamazaki T, Liu Z, Meng D, Kikuta T, Nakatani N, et al. Microstructure and H2 gas sensing properties of undoped and Pd-doped SnO_2 nanowires. Sensors Actuators, B Chem. 2009; 135(2): 524–9.

[74] Hu K, Wang F, Liu H, Li Y, Zeng W. Enhanced hydrogen gas sensing properties of Pd-doped SnO_2 nanofibres by Ar plasma treatment. Ceram Int. 2020; 46(2): 1609–14.

[75] Kaur J, Kumar R, Bhatnagar MC. Effect of indium-doped SnO_2 nanoparticles on NO_2 gas sensing properties. Sensors Actuators, B Chem. 2007; 126(2): 478–84.

[76] Salehi A, Gholizade M. Gas-sensing properties of indium-doped SnO_2 thin films with variations in indium concentration. Sensors Actuators, B Chem. 2003; 89(1–2): 173–9.

[77] D'Arienzo M, Armelao L, Cacciamani A, Mari CM, Polizzi S, Ruffo R, et al. One-step preparation of SnO_2 and Pt-doped SnO_2 as inverse opal thin films for gas sensing. Chem Mater. 2010; 22(13): 4083–9.

[78] Ivanov P, Llobet E, Vilanova X, Brezmes J, Hubalek J, Correig X. Development of high sensitivity ethanol gas sensors based on Pt-doped SnO_2 surfaces. Sensors Actuators, B Chem. 2004; 99(2–3): 201–6.

[79] Dong KY, Choi JK, Hwang IS, Lee JW, Kang BH, Ham DJ, et al. Enhanced H2S sensing characteristics of Pt doped SnO_2 nanofibers sensors with micro heater. Sensors Actuators, B Chem. 2011; 157(1): 154–61.

[80] Kou X, Wang C, Ding M, Feng C, Li X, Ma J, et al. Synthesis of Co-doped SnO_2 nanofibers and their enhanced gas-sensing properties. Vol. 236, Sensors and Actuators, B: Chemical. Elsevier B.V. 2016; 425–432.

[81] Guan Y, Wang D, Zhou X, Sun P, Wang H, Ma J, et al. Hydrothermal preparation and gas sensing properties of Zn-doped SnO 2 hierarchical architectures. Sensors Actuators, B Chem. 2014; 191: 45–52.

[82] Ding X, Zeng D, Xie C. Controlled growth of SnO_2 nanorods clusters via Zn doping and its influence on gas-sensing properties. Sensors Actuators, B Chem. 2010; 149(2): 336–44.

[83] Kolhe PS, Koinkar PM, Maiti N, Sonawane KM. Synthesis of Ag doped SnO_2 thin films for the evaluation of H2S gas sensing properties. Phys B Condens Matter. July 2017; 524: 90–6.

[84] Khudiar AI, Oufi AM. Influence of the aluminium doping on the physical and gas sensing properties of SnO_2 for H2 gas detection. Sensors Actuators, B Chem. 2021; 340(October 2020): 129633.

[85] Wu Y, Zhang H, Liu Y, Chen W, Ma J, Li S, et al. Synthesis and gas sensing properties of single la-doped SnO_2 nanobelts. Sensors (Switzerland). 2015; 15(6): 14230–40.

[86] Hung CM, Phuong HV, Van Thinh V, Hong LT, Thang NT, Hanh NH, et al. Au doped ZnO/SnO_2 composite nanofibers for enhanced H2S gas sensing performance. Sensors Actuators, A Phys. 2021; 317(July 2020): 112454.

[87] Kou X, Meng F, Chen K, Wang T, Sun P, Liu F, et al. High-performance acetone gas sensor based on Ru-doped SnO_2 nanofibers. Sensors Actuators B Chem. 2020; 320: 128292.

[88] Du L, Li H, Li S, Liu L, Li Y, Xu S, et al. A gas sensor based on Ga-doped SnO_2 porous microflowers for detecting formaldehyde at low temperature. Chem Phys Lett. 2018; 713: 235–41.

[89] Jiang Z, Zhao R, Sun B, Nie G, Ji H, Lei J, et al. Highly sensitive acetone sensor based on Eu-doped SnO_2 electrospun nanofibers. Ceram Int. 2016; 42(14): 15881–8.

[90] Inderan V, Arafat MM, Kumar S, Haseeb ASMA, Jiang Z-T, Altarawneh M, et al. Study of structural properties and defects of Ni-doped SnO 2 nanorods as ethanol gas sensors. Nanotechnology. 30 Jun 2017; 28(26): 265702.

[91] Zhang Z, Yin C, Yang L, Jiang J, Guo Y. Optimizing the gas sensing characteristics of Co-doped SnO_2 thin film based hydrogen sensor. J Alloys Compd. 2019; 785: 819–25.

[92] Lian X, Li Y, Tong X, Zou Y, Liu X, An D, et al. Synthesis of Ce-doped SnO_2 nanoparticles and their acetone gas sensing properties. Appl Surf Sci. 2017; 407: 447–55.

[93] Kamble DL, Harale NS, Patil VL, Patil PS, Kadam LD. Characterization and NO_2 gas sensing properties of spray pyrolyzed SnO_2 thin films. J Anal Appl Pyrolysis. 2017; 127(2): 38–46.

[94] Ying Z, Wan Q, Song ZT, Feng SL. SnO_2 nanowhiskers and their ethanol sensing characteristics. Nanotechnology. 2004; 15(11): 1682.

[95] Alhadi A, Ma S, Yang T, Pei S, Yun P, Abbakar KA, et al. Pure SnO_2 Gas Sensor with High Sensitivity and Selectivity towards C2H5OH. Adv Nanoparticles. 2021; 10(02): 66–74.

[96] Khuspe GD, Navale ST, Bandgar DK, Sakhare RD, Chougule MA, Patil VB. SnO_2 nanoparticles-modified polyaniline films as highly selective, sensitive, reproducible and stable ammonia sensors. Electron Mater Lett. 2014; 10(1): 191–7.

[97] Srivastava JK, Pandey P, Mishra VN, Dwivedi R. Sensing mechanism of Pd-doped SnO_2 sensor for LPG detection. Solid State Sci. 2009; 11(9): 1602–5.

[98] Ghimbeu CM, Lumbreras M, Siadat M, van Landschoot RC, Schoonman J. Electrostatic sprayed SnO_2 and Cu-doped SnO_2 films for H2S detection. Sensors Actuators, B Chem. 2008; 133(2): 694–8.

[99] Zhang S, Zhang P, Wang Y, Ma Y, Zhong J, Sun X. Facile Fabrication of a Well-Ordered Porous Cu-Doped SnO 2 Thin Film for H 2 S Sensing. ACS Appl Mater Interfaces. 2014; 6(17): 14975–80.

[100] Salehi A. Selectivity enhancement of indium-doped SnO_2 gas sensors. Thin Solid Films. 2002; 416(1–2): 260–3.

[101] Liu L, Guo C, Li S, Wang L, Dong Q, Li W. Improved H2 sensing properties of Co-doped SnO_2 nanofibers. Sensors Actuators, B Chem. 2010; 150(2): 806–10.

[102] Khuspe GD, Sakhare RD, Navale ST, Chougule MA, Kolekar YD, Mulik RN, et al. Nanostructured SnO_2 thin films for NO2 gas sensing applications. Ceram Int. Dec 2013; 39(8): 8673–9.

[103] Shen Y, Yamazaki T, Liu Z, Meng D, Kikuta T. Hydrogen sensors made of undoped and Pt-doped SnO_2 nanowires. J Alloys Compd. 2009; 488(1): 21–5.